Research Article

SOHAG JOURNAL OF SCIENCES

https://doi.org/10.21608/sjsci.2024.246871.1143

Biosynthesis of Fe_2O_3 and CuO Nanoparticles and Comparative Study for Dielectric Properties

A. A. Hosny[1,*], Bahig El-Deeb[2], Z.A. Mohamed[2], E.M.M. Ibrahim[1]

[1] *Physics Department, Faculty of Science, Sohag University, Sohag 82524, Egypt*
[2] *Botany & Microbiology Department, Faculty of Science, Sohag University, Sohag 82524, Egypt*
[*] *Email: a.h.ahmed@science.sohag.edu.eg*

Received: 6th November 2023 **Revised:** 20th December 2023 **Accepted:** 18th January 2024
Published online: 24th February 2024

Abstract: The present work reports the successful natural synthesis of Fe_2O_3 and CuO nanoparticles (NPs) using sugarcane juice as a reducing and capping agent. The good crystallinity and functional groups of these NPs have been confirmed by x-ray diffraction and Fourier transform infrared spectroscopy, respectively. Besides, the average crystallite size has been calculated to be 18.73 and 16.6 nm for Fe_2O_3 and CuO NPs, respectively. Scanning Electron Microscopy investigation showed nanostructures with irregular shapes of randomly oriented particles. The dielectric properties have been studied at room temperature within the frequency range from 4 kHz to 1 M Hz. Typical behavior of the dielectric constant, dielectric loss, and total conductivity upon varying the applied frequency has been observed. CuO NPs have high dielectric properties and conductivity as compared to Fe_2O_3 NPs. The results revealed that Fe_2O_3 and CuO NPs are promising candidates for use in various applications including energy storage devices, gas sensors and communication systems.
Keywords: Biosynthesis, CuO, Fe_2O_3, dielectric, NPs.

1. Introduction

Recently, nanotechnology nanotechnology-based applications have been widely used in many aspects of life which induces strong motivation to innovate novel synthesis methods of materials on nanosized scale. Among various synthesis methods, green methods are hot topics for now because they offer a high degree of safety, biocompatibility, cost-effectiveness, and simplicity [1]. In contrast, conventional methods require intensive energy, toxic chemicals, and complicated conditions and cause harmful on the ecosystem [2]. Green synthesis is a redox interaction for the involved metal ions using natural and biocompatible materials (e.g. Bacteria, fungi, algae, enzymes, plant extracts) as reducing and stabilizing agents [3]. Various metals and metal oxides nanostructures (NSs) such as Ag [4] Au [5], Pd [6], Pt [7], ZnO [8], Ti_2O [9], CuO [10], and Fe_3O_4 [11] have been successfully synthesized using biological materials. In particular, Fe_2O_3 and CuO are transition metal oxides that have unique properties that nominate them for many promising applications in electronic devices, energy storage, catalysis, pollutants remediation, and biomedicine [12].

Sugarcane is the largest crop production in the world, particularly in African countries[13]. Sugarcane juice (SCJ) (Saccharum officinarum) is a very rich source of reducing agents such as sucrose, fructose, protein substances, and amino acids [14, 15]. Noteworthy, a few studies have investigated the potential reducing capability of SCJ in the green synthesis of nanostructures (NCs) of different materials. This work presents a successful attempt to use SCJ as a reducing and stabilizing agent for the production of Fe_2O_3 and CuO nanoparticles (NPs).

2. Materials and methods

2.1 Biosynthesis of iron and copper oxide nanoparticles

Fresh sugarcane juice was obtained from a local vendor and was filtered using a Whatman filter paper no. 41 to remove dust/solid particles. To synthesize iron oxide NPs, 6 ml of filtered SCJ was mixed with 10 ml of 100 mM $Fe_2(NO)_3.6H_2O$ (LOBA Chemie 99.4%) in 250 ml-glass bottles and stirred thoroughly at 50 °C for 1h. The change of solution color from light brown to dark brown indicates the formation of Fe_2O_3. Similarly, copper oxide NPs were synthesized by adding 5 ml of 100 mM Cu $(NO_3)_2{\cdot}3H_2O$ (LOBA Chemie 99.5%) to 6 ml filtered SCJ with stirring at 50°C for 30 min. The color changed from blue to green indicates the successful formation of CuO NPs. Simultaneously, the experiment was carried out with the same procedures but without SCJ, and the solution was kept as a control. The control solution remained without any color change. The pH was kept at 10 during the stirring by adding NaOH dropwise. Both control and SCJ reaction solutions were incubated for 24 h at room temperature. Double distilled water was used as a solvent in all reactions. To remove the free nitrate ions and organic impurities, the obtained precipitates were centrifuged and thoroughly washed with distilled water, and placed in a hot air oven at 60 °C for 24 h to obtain a dry powder. Then, the dried Fe_2O_3 and CuO powders were sintered at 600 and 400 °C for 6 and 4 h, respectively in a muffle furnace.

2.2 Materials characterization

2.2.1. X-ray diffraction (XRD)

X-ray powder diffraction (XRD) measurements were carried out using a D8-Advance, Bruker diffractometer with Cu-Kα radiation (λ= 1.54 Å), within 2θ collection range of 20–80° with an angle step size of 0.02°. The average crystallite size (D) was estimated from the XRD patterns using Debye–Scherrer formula[16]:

$$D = \frac{K\,\lambda}{\beta cos\theta} \quad (1)$$

where D is the crystallite size, *K* is a constant related to the crystallite shape (*K*=0.9), λ is the wavelength of the Cu-Kα radiation, β is the full width at half maximum (FWHM) of the most predominant peaks (in radians) and θ is the diffraction angle (in radians).

The lattice parameters (*a*,*b*,*c*, and β) and cell volume were calculated for the monoclinic structure of CuO using the following equations[17]:

$$\frac{1}{d^2} = \frac{1}{sin^2\,\beta}\left(\frac{h^2}{a^2} + \frac{k^2\,sin^2\,\beta}{b^2} + \frac{l^2}{c^2} - \frac{2hl\cos\beta}{ac}\right) \quad (2)$$

$$V = abc\ \ sin\,\beta \quad (3)$$

The relations used for determining Lattice parameters and cell volume for hexagonal Fe_2O_3 structure are[18]:

$$\frac{1}{d^2} = \frac{4}{3}\left(\frac{h^2+hk+k^2}{a^2}\right) + \frac{l^2}{c^2} \quad (4)$$

$$V = 0.866a^2c \quad (5)$$

The micro strain (η) and dislocation density (δ) for both Fe_2O_3 and CuO samples were calculated to indicate the amount of deformations in a lattice structure by using equations[19]:

$$\eta = \frac{\beta_{hkl}\cos\theta}{4} \quad (6)$$

$$\delta = \frac{1}{D^2} \quad (7)$$

2.2.2. Fourier Transform Infra-Red (FTIR) spectra:

Fourier Transform Infra-Red spectra (Alpha FTIR Bruker in Sohag University, Egypt) for SCJ, Fe_2O_3, and CuO powders were recorded to investigate the chemical functional groups of the surface.

2.2.3. Scanning Electron Microscopy (SEM)

Morphological features of the biosynthesized oxides were investigated by the field emission scanning electron microscope FESEM model ZEISS-Sigma 500 FE-SEM).

2.2.4. Dielectric properties

Room temperature dielectric measurements were conducted within the frequency range from 4kHz to 1 MHz using the Hioki LCR meter model IM 3536 LCR METER. The dielectric constant, dielectric loss, and conductivity were monitored directly from the LCR meter as functions of the applied frequency.

3. Results and Discussion:

3.1 Structural properties

The formation of iron oxide and copper oxide NPs is confirmed by XRD investigation. For biosynthesized iron oxide (Fig. 1a), the observed Bragg peaks (2θ˚(hkl)) 24.1° (102), 33.2° (104), 35.7° (110), 40.7° (113), 49.5° (204), 54° (116), 57.5° (108), 62.58° (214), 71.9° (1010) correspond to the hexagonal hematite α-Fe_2O_3 crystalline phase (according to COD 2101167card). It must be noted that in iron oxides, the differentiation between α-Fe_2O_3, Fe_3O_4, and γ- Fe_2O_3 is very difficult by XRD investigation because of very similar d-space values **[20, 21]**. Fig. 1b illustrates the XRD pattern of the biosynthesized CuO NPs. The characteristic peaks at (2 θ°) 32.5°, 35.44°, 38.67°, 48.85°, 53.3°, 58.32°, 61.5°, 66.2°, 68.03°, 72.3°, and 75.04°, corresponding to (hkl) (110), (11-1), (111), (20-2), (020), (-113), (31-1), (220), (311), and (004) planes, respectively are identified as pure phase of crystalline monoclinic structure of CuO in coincidence with COD card No. 9016105.

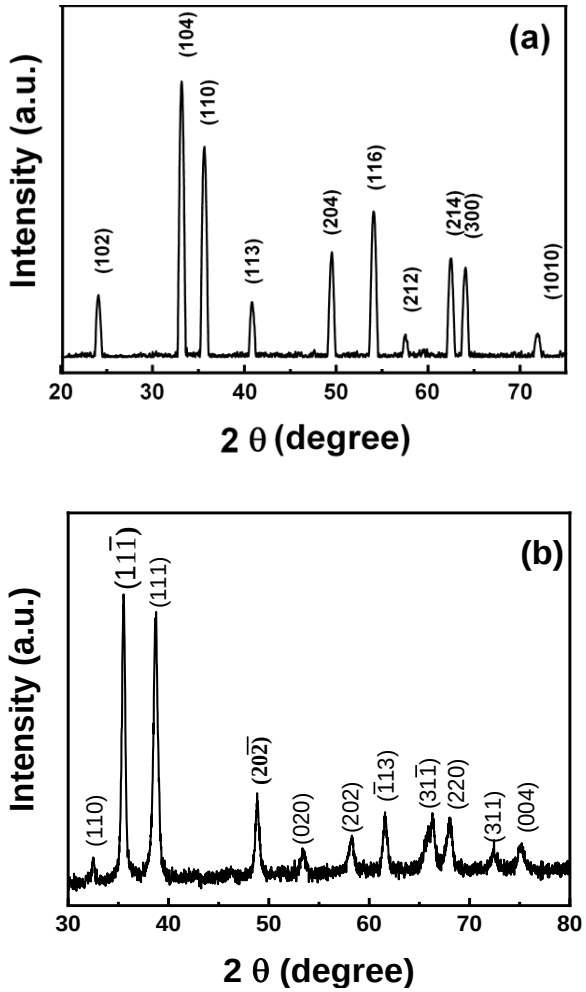

Figure 1: XRD pattern for biosynthesized a) Fe_2O_3, b) CuO NPs.

The average crystallite size (*D*) for Fe_2O_3 and CuO NPs were determined using the Debye–Scherrer formula (Eq.1) to be 18.73 and 16.6 nm, respectively. The lattice constants (a, b and c) and cell volume (V) were determined using Eqs. 2 & 3 for CuO and Eqs. 4 & 5 for Fe_2O_3. Also, the dislocation density (δ) and micro-strain (η) were estimated by Eqs. 6 & 7, respectively. The values were tabulated in Table 1. The data (see Table 1) imply a good match with the standard values for α-Fe_2O_3[22]and for CuO **[23, 24].**

The functional chemical groups found in SCJ, and the resultant Fe_2O_3, and CuO NPs are investigated by the FTIR spectrum in the range of 400–4000 cm^{-1} (Fig. 2). There are five characteristic peaks common in SCJ sample noticed around 3352, 2873, 1639, 1060, and 596 cm^{-1} correspond to hydroxyl group O-H, C-H stretch group, C=O stretch group, O-C=O, and bending vibration =C–H, respectively [25, 26]. On the other hand, there are similar peaks in biosynthesized samples but with different intensities. In addition, the peaks from 400-500 cm^{-1} correspond to the stretching vibration mode of Fe–O, and Cu-O in Fe_2O_3 and CuO samples respectively [25]. FTIR results suggest the presence of sucrose, fructose, and other biomolecules namely, amino acids and organic acids on the surface of resultant NPs, working as capping agents [26-28].

Table 1: Lattice parameters, cell volume (V) dislocation density (δ), and micro strain (η) of Fe_2O_3 and CuO.

Lattice parameters	α-Fe_2O_3	CuO
a (Å)	5.02±0.002	4.68±0.0021
b (Å)	-	3.42±0.0019
C(Å)	13.73±0.008	5.12±0.0019
V (Å)	300.09±0.3	81.01±0.06
Dislocation density δ (Line/nm^2)	0.00285	0.002621
Micro-strain η	0.001944	0.002206

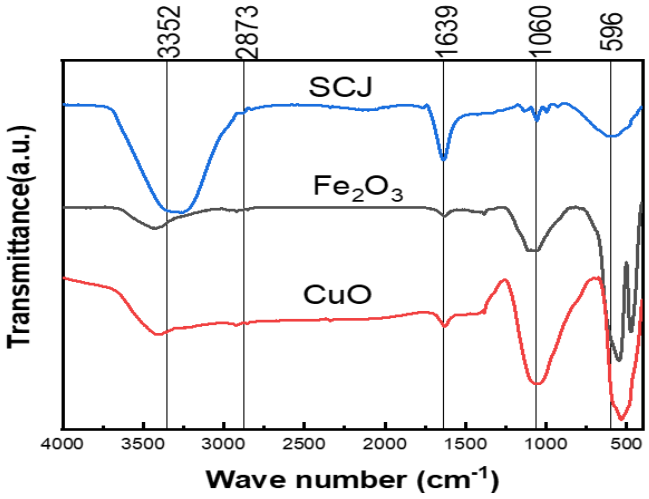

Figure 2: FT-IR spectra for SCJ, biosynthesized Fe_2O_3, and CuO NPs.

3.2 Morphological study

Fig. 3 depicts the FE-SEM images of the synthesized materials. The images illustrate that both Fe_2O_3 and CuO samples consist of randomly oriented nano-sized particles with irregular hexagonal-like and spherical shapes respectively. The average size of Fe_2O_3 and CuO NPs was estimated to be 189 and 33.3 nm, respectively. Noteworthy, the estimated average particle size determined from SEM imaging is higher than the value of crystallite size D determined from the X-ray patterns because the particle can consist of many crystallites.

3.3 Dielectric studies

Dielectric measurements are essential for monitoring the mechanisms of polarization, the process of conduction, and roles of defects in a material lattice. Accordingly, the dielectric constant and dielectric loss are measured to identify the dielectric behavior of the synthesized Fe_2O_3 and CuO. The dielectric constant is a complex parameter given as [18]:

$$\varepsilon^* = \varepsilon' - i\varepsilon'' \quad (8)$$

where ε′ and ε″ are the real and imaginary components of the complex dielectric function and they are related by the loss tangent, tan δ from the formula [19]:

$$tan\,\delta = \frac{\varepsilon''}{\varepsilon'} \quad (9)$$

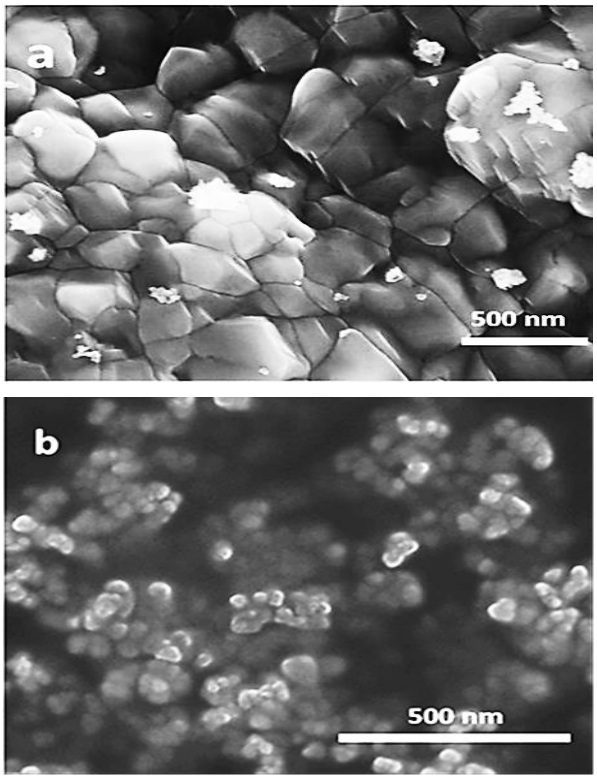

Figure 3: FSEM images for biosynthesized Fe_2O_3 (a) and CuO (b).

Fig.4 illustrates the variation of room temperature dielectric constant (real part) ε′ with frequency. ε′ behavior for both samples shows an exponential-like plot with the highest values at low frequencies and decreases with the increase in frequency showing approximately constant values in the high frequency range. It is worth mentioning that, many types of polarization occur in the polar materials including ionic, electronic, orientational, and space charge polarization [16]. Since the first two types of polarization are effective in the infrared and above-infrared frequency ranges, the polarization within the studied range of frequencies may originate from the space charge and orientational polarizations[18, 21]. The space charge polarization originates due to the existence of highly electrical conductive grains inside the materials separated by the low electrical conductive grain boundaries [15]. According to Koops 'model, the freely moved charge carriers accumulate on the

interface between the grain and grain boundary particularly at low frequencies [29]. The orientation polarization is caused by the orientation of the dipoles formed by the oxygen ions and oxygen vacancies at the interfaces in the presence of an electric field[30]. So, the observed high values of ε′ at low frequency could be attributed to the space-charge polarization and dipole orientation. However, as the frequency increases, ε′ decreases due to the mismatch between the dipole's alignment and the applied electric field where the dipoles become unable to follow the change in the applied field direction [24]. Similar behavior of the dielectric loss ε″ with frequency is observed in Fig. 4. Dielectric loss ε″ refers to energy dissipation in the dielectric materials upon applying the electric field. The studies revealed that conduction and relation polarizations contribute largely to the losses of energy [16]. The values of ε″ of the biosynthesized iron and copper oxide NPs indicate that they are promising candidates for use in energy storage devices. Fig. 5 reveals the conductivity variation with frequency measured at room temperature. The measured conductivity is the sum of both DC and AC components which predominate at low and high-frequency ranges, respectively[30, 31]. It is observed that the conductivity of Fe_2O_3 NPs increased steadily, indicating the absence of the DC conductivity contribution at the low frequency range which can be attributed to the limited motion of the free charge carriers in iron oxide. The increase in the conductivity with frequency is related to the domination of the AC conductivity (σ_{ac}) and is well represented by Jonscher's law ($\sigma_{ac}=A\ \omega^s$, where *A* and *s* are the proportionality constant and the frequency exponent)[24]. According to Jonscher's model, the improvement in the AC electrical conductivity is caused by the increase in the rate of charge carrier hopping between defects created in the material. The CuO conductivity showed a slight increase at low frequency range due to DC conductivity contribution resulting from the higher content of the charge carriers and their ability to transfer in the material. At high frequency, the conductivity increases significantly upon increasing the frequency, indicating domination of the AC conductivity where the electrons hopping increases. Similar data for CuO NPs were reported by previous studies[32].

4. Conclusion

Green biosynthesis of nanoparticles using sugarcane juice is a successful method to fabricate well crystalline and pure iron oxide and copper oxide nanostructures without using toxic chemicals as reducing agents. The high-purity crystalline structure of these nanoparticles is confirmed by XRD analysis. The crystallite size was found to be 16.6 nm for iron oxide and 18.73 nm for copper oxide NPs. Also, FTIR analysis indicates that some biomolecules in sugarecane juice such as sucrose, fructose, and protein substances may be responsible for the reduction process and act as capping agents on the surface. CuO NPs have high dielectric constant ε′ and dielectric loss ε″ as compared to Fe_2O_3 NPs. The space charge and orientational polarizations are the most contributions to the dielectric behavior on the applied frequency range. Similarly, the higher conductivity for CuO NPs concerning Fe_2O_3 NPs refers to the higher concentration of charge carriers. So, these traits of produced NPs make them promising candidates for application in energy storage and communication devices. Additionally, the biosynthesized Fe_2O_3 and CuO NPs merit deeper investigation in further study.

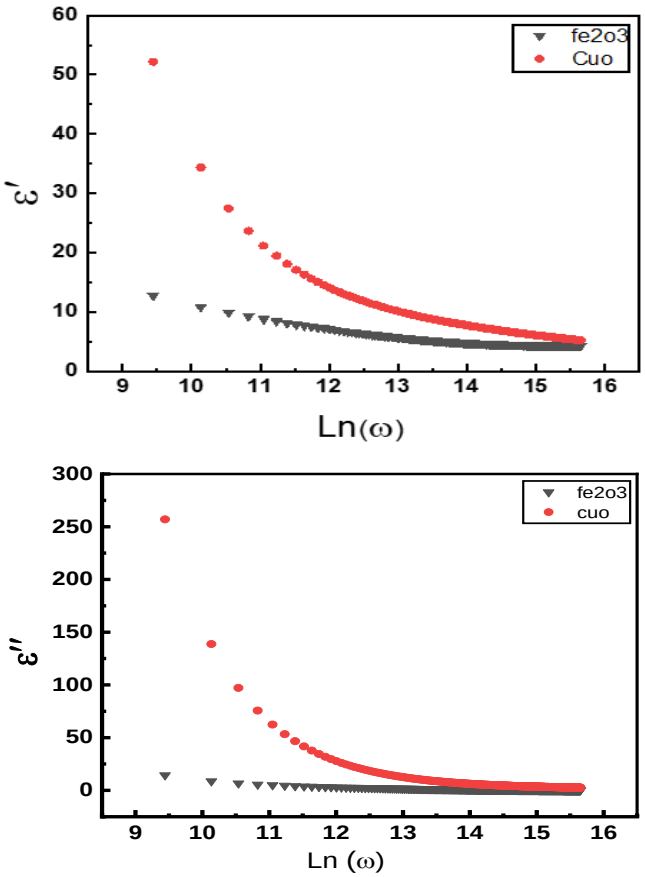

Figure 4: The variation of dielectric constant ε′ and dielectric loss ε″ for Fe_2O_3 and CuO NPs with frequency at room temperature.

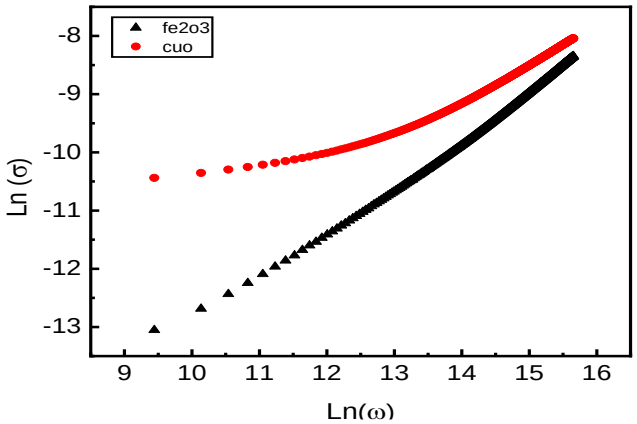

Figure 5: The variation of conductivity of Fe_2O_3 and CuO NPs with frequency at room temperature.

CRediT authorship contribution statement:

Conceptualization, A.A. Hosny , E.M.M. Ibrahim, Bahig El-Deeb, Z.A. Mohamed; methodology, A.A. Hosny;

validation, E.M.M. Ibrahim, Bahig El-Deeb, and Z.A. Mohamed; investigation, E.M.M. Ibrahim, Bahig El-Deeb, and Z.A. Mohamed; data curation, E.M.M. Ibrahim, and A.A. Hosny; writing—original draft preparation, A.A. Hosny; writing—review and editing, E.M.M. Ibrahim, Bahig El-Deeb, Z.A. Mohamed; visualization, E.M.M. Ibrahim, Bahig El-Deeb,and Z.A. Mohamed; supervision, E.M.M. Ibrahim, Bahig El-Deeb, Z.A. Mohamed. All authors have read and agreed to the published version of the manuscript.

Data availability statement

The data used to support the findings of this study are available from the corresponding author upon request.

Declaration of competing interest

The authors declare that they have no known competing financial interests or personal relationships that could have appeared to influence the work reported in this paper.

References

[1] H.N. Cuong, S. Pansambal, S. Ghotekar, R. Oza, N.T.T. Hai, N.M. Viet, V.-H. Nguyen, *Environmental Research*, 203 (2022) 111858.
[2] N.T.T. Nguyen, L.M. Nguyen, T.T.T. Nguyen, R.K. Liew, D.T.C. Nguyen, T. Van Tran, *Science of the Total Environment*, 827 (2022) 154160.
[3] N. Zikalala, K. Matshetshe, S. Parani, O.S. Oluwafemi, *Nano-Structures & Nano-Objects*, 16 (2018) 288-299.
[4] C.S. Espenti, K.K. Rao, K.M. Rao, *Materials letters*, 174 (2016) 129-133.
[5] M. Camas, F. Celik, A. Sazak Camas, H.B. Ozalp, *Particulate Science and Technology*, 37 (2019) 31-38.
[6] L.S. Søbjerg, A.T. Lindhardt, T. Skrydstrup, K. Finster, R.L. Meyer, *Colloids and Surfaces B: Biointerfaces*, 85 (2011) 373-378.
[7] S.K. Srivastava, M. Constanti, *Journal of Nanoparticle Research*, 14 (2012) 1-10.
[8] G. Karunakaran, M. Jagathambal, G.S. Kumar, E. Kolesnikov, *Jom*, 72 (2020) 1264-1272.
[9] A. Chinnathambi, S. Vasantharaj, M. Saravanan, S. Sathiyavimal, P.A. Duc, O. Nasif, S.A. Alharbi, N.T.L. Chi, K. Brindhadevi, *Applied Nanoscience*, (2021) 1-8.
[10] N. Asif, R. Ahmad, S. Fatima, S. Shehzadi, T. Siddiqui, A. Zaki, T. Fatma, *Scientific reports*, 13 (2023) 6246.
[11] N.D.S. Zambri, N.I. Taib, F. Abdul Latif, Z. Mohamed, *Molecules*, 24 (2019) 3803.
[12] S. Drummer, T. Madzimbamuto, M. Chowdhury, *Materials*, 14 (2021) 2700.
[13] S. Patil, H.B. Naik, G. Nagaraju, R. Viswanath, S. Rashmi, *Materials Chemistry and Physics*, 212 (2018) 351-362.
[14] A.A. Mary, A.T. Ansari, R. Subramanian, *Journal of King Saud University-Science*, 31 (2019) 1103-1114.
[15] H. Saadallah, A. Abdel Hakeem, S. Saleh, S. Hampel, E. Ibrahim, *Sohag Journal of Sciences*, 8 (2023) 281-287.
[16] H. Nazli, A. Arshad, Z.N. Kayani, A. Razi, *Materials Chemistry and Physics*, 308 (2023) 128222.
[17] P. Chand, P. Kumar, *Optik*, 156 (2018) 743-753.
[18] M. Qayoom, K.A. Shah, A.H. Pandit, A. Firdous, G.N. Dar, *Journal of Electroceramics*, 45 (2020) 7-14.
[19] N. Ahmad, S. Khan, M.M.N. Ansari, *Ceramics International*, 44 (2018) 15972-15980.
[20] E. Ibrahim, S. Hampel, J. Thomas, D. Haase, A. Wolter, V.O. Khavrus, C. Täschner, A. Leonhardt, B. Büchner, *Journal of Nanoparticle Research*, 14 (2012) 1-9.
[21] Y. Li, Z. Wang, R. Liu, *Nanomaterials*, 11 (2021) 834.
[22] J.B. Lee, H.J. Kim, J. Lužnik, A. Jelen, D. Pajić, M. Wencka, Z. Jagličić, A. Meden, J. Dolinšek, *Journal of Nanomaterials*, 2014 (2014) 191.
[23] E. Ibrahim, L.H. Abdel-Rahman, A.M. Abu-Dief, A. Elshafaie, S.K. Hamdan, A. Ahmed, *Materials Research Bulletin*, 107 (2018) 492-497.
[24] Ç. Oruç, A. Altındal, *Ceramics international*, 43 (2017) 10708-10714.
[25] A. Rufus, N. Sreeju, D. Philip, *RSC advances*, 6 (2016) 94206-94217.
[26] L.C. Sim, J.L. Wong, C.H. Hak, J.Y. Tai, K.H. Leong, P. Saravanan, *Beilstein journal of nanotechnology*, 9 (2018) 353-363.
[27] A.S. Dhaulaniya, B. Balan, A. Yadav, R. Jamwal, S. Kelly, A. Cannavan, D.K. Singh, *Food Additives & Contaminants: Part A*, 37 (2020) 539-551.
[28] N. Du, L. Pan, J. Liu, L. Wang, H. Li, K. Li, C. Xie, F. Hang, H. Lu, W. Li, *Membranes*, 12 (2022) 910.
[29] C. Koops, *Physical review*, 83 (1951) 121.
[30] N. Abraham, S. Aseena, *Materials Today: Proceedings*, 43 (2021) 3698-3700.
[31] A.K. Jonscher, *nature*, 267 (1977) 673-679.
[32] A. Pramothkumar, N. Senthilkumar, R.M. Jenila, M. Durairaj, T.S. Girisun, I.V. Potheher, *Journal of Alloys and Compounds*, 878 (2021) 160332.